GEM TN-93-429

Studies on the Reduction of Neutron and Gamma Leakage from the Forward Region of the GEM Detector

Brent R. Moore
University of Mississippi

July 1, 1993

Abstract;

CALOR89 has been used to consider various design aspects of the forward region of the GEM detector in order to minimize neutron and photon leakage from this part of the detector. In particular, escapes from the vacuum gap between the inner and outer crysotat wall, escapes from between the passive absorber and the forward field shaper, and punchthrough of the passive absorber have all been addressed. Some possible solutions that are considered are putting a muon shield between the passive absorber and forward field shaper, optimizing the passive absorber in terms of what materials to use and their thicknesses, and lining the inside of the passive absorber with borated polyethylene.

Studies on the Reduction of Neutron and Gamma Leakage from the Forward Region of the GEM Detector

Brent R. Moore

University of Mississippi

Abstract

CALOR89 has been used to consider various design aspects of the forward region of the GEM detector in order to minimize neutron and photon leakage from this part of the detector. In particular, escapes from the vacuum gap between the inner and outer cryostat wall, escapes from between the passive absorber and the forward field shaper, and punchthrough of the passive absorber have all been addressed. Some possible solutions that are considered are putting a muon shield between the passive absorber and forward field shaper, optimizing the passive absorber in terms of what materials to use and their thicknesses, and lining the inside of the passive absorber with borated polyethylene.

Studies on the Reduction of Neutron and Gamma Leakage from the Forward Region of the GEM Detector

1. Introduction

The leakage of neutrons and of photons resulting from (n, γ) reactions is a particular problem for detectors at the SSC and the LHC. In recognition of this, both GEM and SDC have been evaluating the design of their detectors in order to minimize this leakage. Of particular concern for GEM are the forward region and the focusing quadrupole magnets that are closest to the detector. I have used CALOR89 to consider various design aspects of the forward region of the GEM detector in order to minimize neutron and photon leakage from this part of the detector.

My approach has been to concentrate on doing some rough calculations for the forward region that could be done fairly quickly and to then pass on recommended changes for inclusion in a more global simulation such as LAHET or SIGEM, which uses GCALOR, the GEANT program that includes modules from the CALOR package. The global simulation could then show if the suggested changes caused problems that might have gone undetected in a regional simulation, and could give results on the overall leakage and spectra that can be expected from all sources.

The study was conducted using source particles from 1000 DTUJET minimum bias events of 20 TeV protons on 20 TeV protons. At a luminosity of 10^{33}, there will be approximately 10^8 interactions per second at the SSC. Due to time considerations, one-tenth of these particles were chosen randomly for transport using the simulation code, which should correspond to 100 jet events, so my simulations correspond to one SSC-microsecond. Since CALOR89 cannot transport more exotic particles such as Ξ and Λ, particles such as these were transported as pions having the same charge. This should suffice for rough calculations since the kinetic energy of these particles is much greater than the rest mass energy.

I was concerned about three areas in particular:

- Escapes from the vacuum gap between the inner and outer cryostat wall.

- Escapes from between the passive absorber, which lies just outside the forward hadronic calorimeter, and the forward field shaper.
- Escapes that punch through the passive absorber.

In this paper I consider the following topics in the attempt to solve these problems:

- A muon shield between the passive absorber and the forward field shaper.
- Optimizing the passive absorber in terms of what materials to use and their thicknesses to reduce neutron and photon punchthrough.
- Lining the inside of the passive absorber with borated polyethylene to reduce the neutrons escaping out the cryostat vacuum gap.

Each of the above topics will be considered in a separate section below.

2. Geometry of the Forward Region

Fig. 1 shows the baseline of the GEM calorimeter as it existed in early- to mid-March. The geometry simulated in my CALOR89 runs is shown in Fig. 2. I include the endcap calorimeters in my simulation, starting at $Z = 200$ cm. I include the forward region all the way out to the back of the forward field shaper (FFS), which at that time was at $Z = 1800$ cm. The endcap calorimeters as simulated extend radially out to $R = 196.6$ cm. There was a slight simplification in my geometry in that the hadronic endcap calorimeter which lies outside the electromagnetic endcap calorimeter was ignored, and the electromagnetic calorimeter was extended out to the simulated radius. This should not be a significant deviation from the actual geometry for this particular simulation, since particles which are transverse enough to be in this area will almost always have too little energy and need to penetrate too much material to contribute to the neutron and photon leakage in the forward region. In the area that includes the forward calorimeters and beyond, the detector was simulated out to a radius of $R = 282$ cm.

To better study the effects of different components in the geometrical configuration, I divided the source jet particles into three distinct regions. Those in what I call the 'Front' region lie in a pseudorapidity range of about $2.5 < \eta < 4.4$. These particles strike the

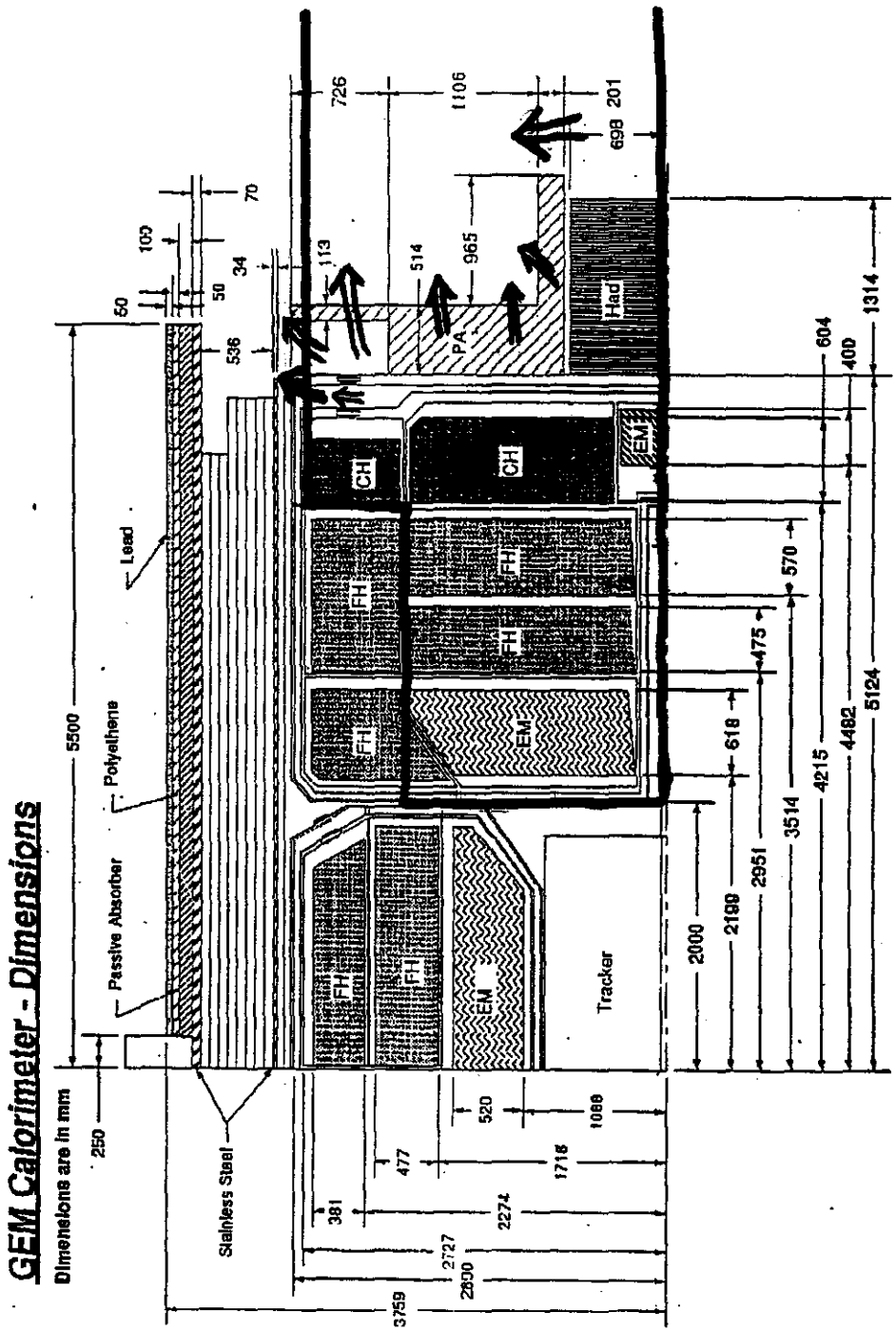

GEM Baseline as of March 1993

Forward Region Simulated is in Bold Line

Arrows Indicate Areas of Concern for Neutron Leakage

FIGURE 1

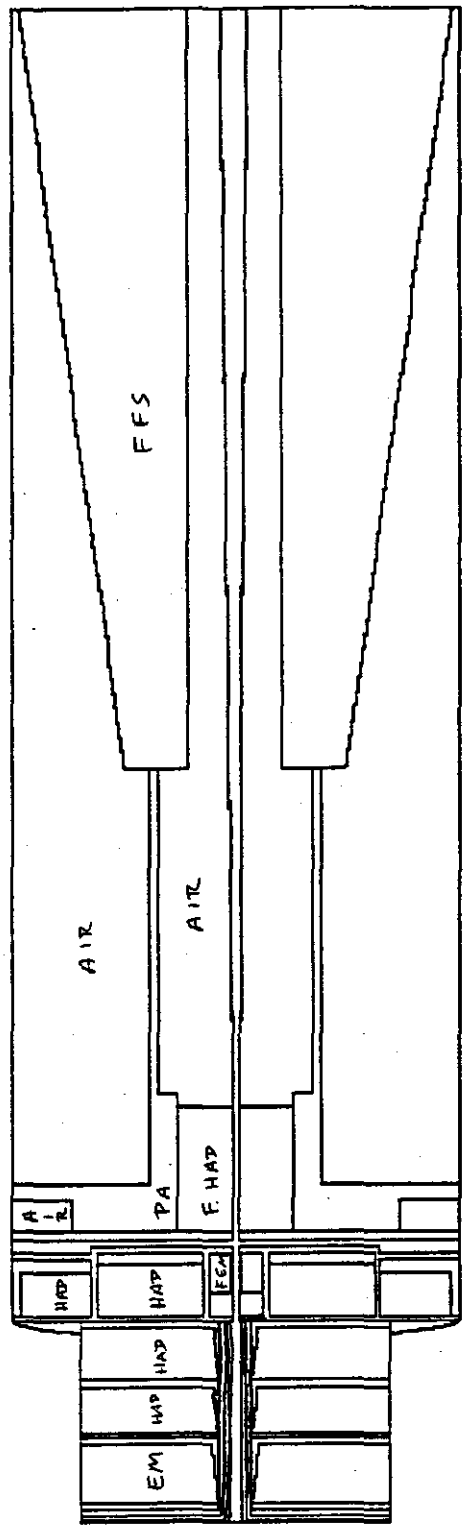

SABRINA Picture of GEM Baseline
as Simulated Using CALOR89

FIGURE 2

endcap calorimeters all the way back to where the beam pipe decreases in radius from 10 cm to 4 cm (Z = 417.8 cm) and strike the front of the endcap calorimeter cryostat as far away from the beam as 33 cm. I refer to the 'Middle' region as lying in the range $4.4 < \eta < 5.6$. These particles strike the vertical wall at the front of the forward cryostat and strike the beam pipe under the forward electromagnetic calorimeter and outer cryostat vacuum gap all the way back to where the forward hadronic calorimeter (FHAC) begins. Particles which strike the beam pipe just underneath the forward hadronic calorimeter are said to be in the 'Back' region and lie in the range of $5.6 < \eta < 5.8$.

Particles with $\eta < 2.5$ are too transverse to have significant energy to punch through the greater thickness of material that is required, so these were not transported. Immediately behind the forward hadronic calorimeter, the beam pipe flares out so as to lie completely in the shadow of the calorimeter, so those jet particles with $\eta > 5.8$ miss the forward region entirely and don't interact until they reach the collimator area. Thus only those particles in the range $4.4 < \eta < 5.8$ were of interest to us. This pseudorapidity range has about 4% of the jet energy, or around 0.8 TeV.

In my simulated geometry of the baseline, a muon shield of 10 cm thick copper lies just outside the flange of the passive absorber (it appears to be on top of it in a two-dimensional cutaway of the detector) and extends on back to the FFS.

3. The Shield Between the Passive Absorber and the Forward Field Shaper

Fig. 3 shows the number of neutrons escaping the baseline in the upper half and a modified baseline configuration with an enhanced muon shield in the lower half. The numbers shown are the neutrons escaping from three surfaces which are entering the area where the forward muon chambers are.

There are 4183 neutrons escaping out the surface of constant radius at R = 282 cm from the front of the most forward endcap hadronic calorimeter back to the back surface of the passive absorber (PA). Almost all of these particles are escaping through the vacuum gap between the inner and outer cryostat wall. Of these 4183 neutrons, about two-thirds of them come from jet particles in the Middle region, which includes those that strike

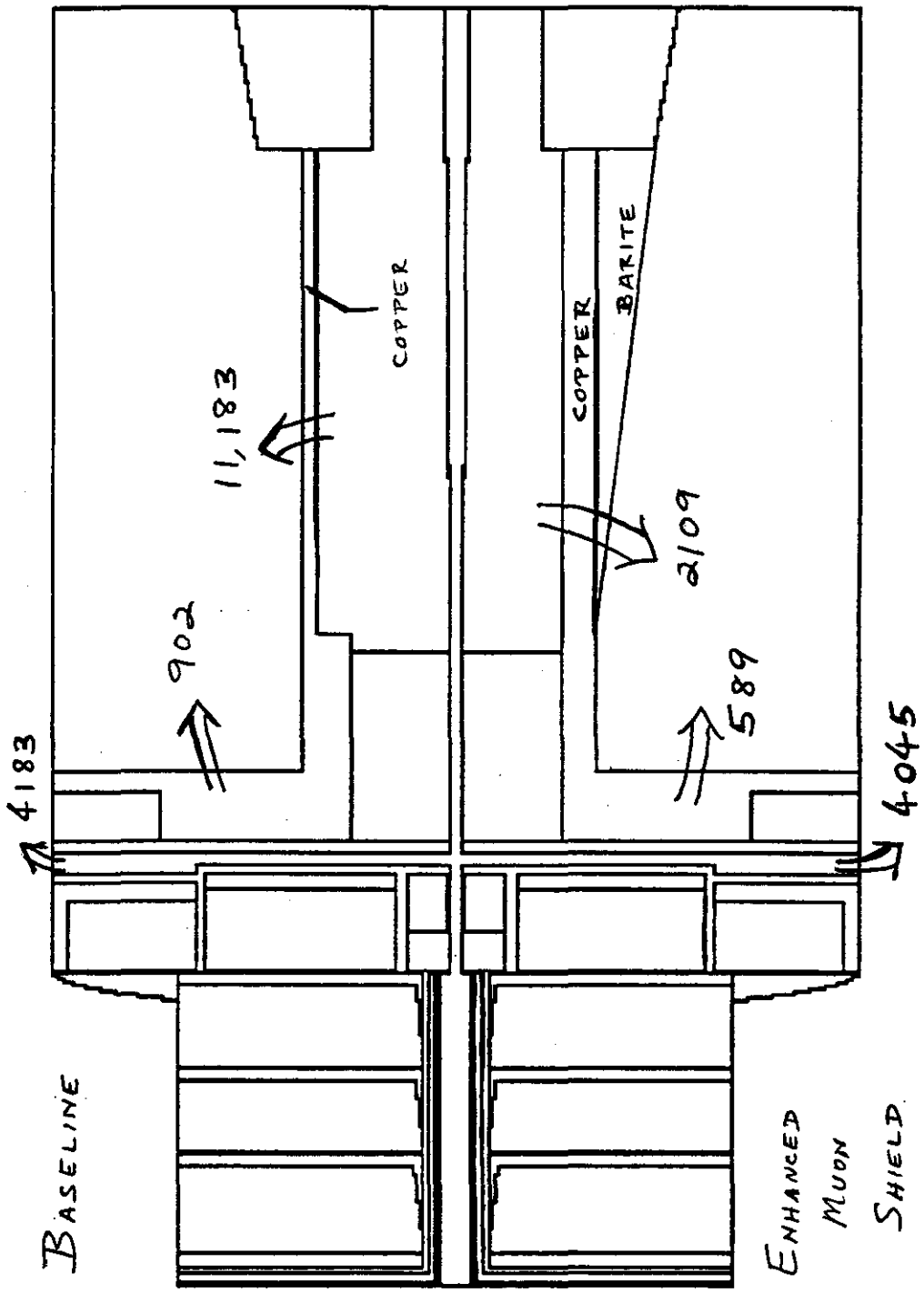

Neutron Escapes from Areas of Concern

Upper Half - Baseline Configuration

Lower Half - Baseline with Enhanced Muon Shield

FIGURE 3

the beam pipe just inside this vacuum gap. Some of the neutrons escaping here may be absorbed by the scintillating barrel calorimeter or other material outside the cryostat, but a number of them can be expected to be reflected toward the forward muon chambers.

The particles exiting the back of the PA number 902. By studying the location, direction of travel, age, and energy of the neutrons crossing this surface in both directions, I have determined that about 65% of these are actually neutrons which entered the PA from behind and were reflected back. So roughly just over 300 of these actually punched through to the back of the PA.

The largest source of neutrons leaking into the forward muon chamber (FMC) region was leakage coming out of the gap that extends from the back of the PA back to the FFS. There were 11,183 neutrons crossing through the 10 cm thick copper muon shield. About 80% of these were from jet particles in the Back region – those that strike inside the forward calorimeter. These are evidently reflecting out to the muon shield, and perhaps off the front of the FFS, as well.

These neutrons represent over half of all the neutrons entering the FMC region. Were it possible to make the inside of the FHAC projective, all the jet particles striking inside the FHAC would instead miss this calorimeter and go all the way back to the collimator where they could perhaps be better dealt with. Except for some small percentage of the neutrons bouncing back from the collimator region, this would eliminate all the neutrons coming from jet particles in the Back region.

With this source eliminated for the baseline, the neutrons escaping the cryostat vacuum gap number 4067, an insignificant difference; the neutrons crossing the back of the PA are 448, a reduction of about 50%; and the number of neutrons escaping between the PA and the FFS are 2265, down by a factor of five. Overall, the number of neutrons decreases by about 60% when the FHAC is made projective. Unfortunately, difficulties involved in making the FHAC projective prevent this from being an option. There is another solution, however, which simulations indicate is as good or better.

The bottom half of Fig. 3 shows the modified baseline with the enhanced muon shield. The 10 cm thick copper shield that lies just outside the PA flange has been removed. Present instead is a copper cylinder which extends the flange on back all the way to the

FFS and which is about 25 cm thick. A hollow, truncated cone (looks like a wedge in the cutaway drawing) of barite concrete lies outside this copper shield, beginning where the PA flange stopped before and extending outward to the outer edge of the front face of the FFS. This makes it about 41 cm thick at the FFS ($Z = 1000$ cm).

The barite concrete is about 40% barium by weight, 1% boron and 0.8% hydrogen. Of course, since hydrogen is very light, there is nonetheless a relatively large number of hydrogen nuclei present in the concrete. The hydrogen helps to slow down neutrons that have energy of about 5 MeV or below, and the boron is quite effective at absorbing them in this energy range. The thick layer of copper is helpful in absorbing some high energy neutrons and in slowing down others so that they are in the range of about 5 MeV where the neutron scattering cross section for hydrogen is more significant. Thus, it makes perfect sense to put the copper on the inside and the barite concrete on the outside. The barite concrete, with a density of $3.2\frac{g}{cm^3}$, has an added advantage of being much lighter than other absorbers such as copper or iron.

As expected, the leakage out the cryostat vacuum gap is essentially unchanged by putting in this shield. The simulation with the enhanced shield now has 4045 neutrons escaping out the surface at $R = 282$ cm. The decrease from 4183 is insignificant.

The number of neutrons leaving the back surface of the PA is decreased to 589, of which about 40% can be seen to be reflections from behind the PA. This means that the number of reflected particles has been about cut in half, from the upper 500's to the lower 200's. The number of punchthrough neutrons has actually increased very slightly, from the lower to the mid 300's. The reason for this is simply that the back of the PA now covers a greater area – extending radially inward to the PA flange instead of being 10 cm further out because of the copper cylinder in the baseline.

As expected, the biggest change with the enhanced muon shield is a significant decrease in the number of neutrons escaping between the PA and the FFS from 11,183 to 2109. About two-thirds of these, 1373, come from jet particles in the Back region. So the number of neutrons escaping from this gap is decreased by a factor of over five by using the larger muon shield, and the largest source of neutrons is now the cryostat vacuum gap.

Overall, inclusion of the muon shield reduces the number of escaping neutrons from

16,268 to 6743 – a total reduction of about 60%. This number compares favorably to 6780, which was the number of escaping neutrons for the baseline if all the jet particles striking the inside of the FHAC could be eliminated by making the FHAC projective on the inside.

Fig. 4 shows plots of the neutron flux at the outside of the muon shield between the PA and FFS for the baseline and for the enhanced shield. The barite concrete wedge in the enhanced shield begins at $Z = 657.1$ cm. We see that the flux with the enhanced muon shield decreases steadily as one moves further from the interaction point and toward the FFS where the barite shield is thickest. From $Z = 850$ cm and out, the flux is decreased by $1\frac{1}{2} - 2$ orders of magnitude. Even just outside the forward hadronic calorimeter, which extends only out to $Z = 643.8$ cm, the neutron flux is reduced significantly, perhaps indicating that much of the flux here in the baseline case is due to reflection off the FFS which is diminished by the barite wedge in the case of the enhanced muon shield. Note that the flux in the baseline is typically around 6×10^{11} neutrons/cm^2/SSC-year in the gap between the PA and FFS. This is in agreement with the numbers of 10^{11} to 10^{12} that have been established by Laurie Waters using LAHET and by Yuri Fisyak using the SIGEM implementation of GCALOR.

I also investigated some other geometrical configurations. For instance, if the cryostat vacuum gap is filled with copper, the total number of neutrons escaping in this region plummets to 209 – a reduction by a factor of twenty. Of course, filling this gap with copper is not an option in the actual design, but this does give us an idea of the best one can possibly do with modified designs that somewhat diminish the gap.

4. Optimization of the Passive Absorber for Punchthrough Reduction

Fig. 5 shows the neutron flux at the back of the PA for the baseline configuration. Notice that the flux is greatest at the inside radius of the PA. A block of material (actually a ring in three-dimensions that looks like a block in the cutaway view) at the inner radius of the PA, placed just against the PA flange, should have a significant impact in cutting down the neutron flux and reducing the number of neutrons leaking into the FMC region.

I have conducted a number of runs to check the impact of using different materials in the PA and of varying their thicknesses. The simulations used the geometry shown in

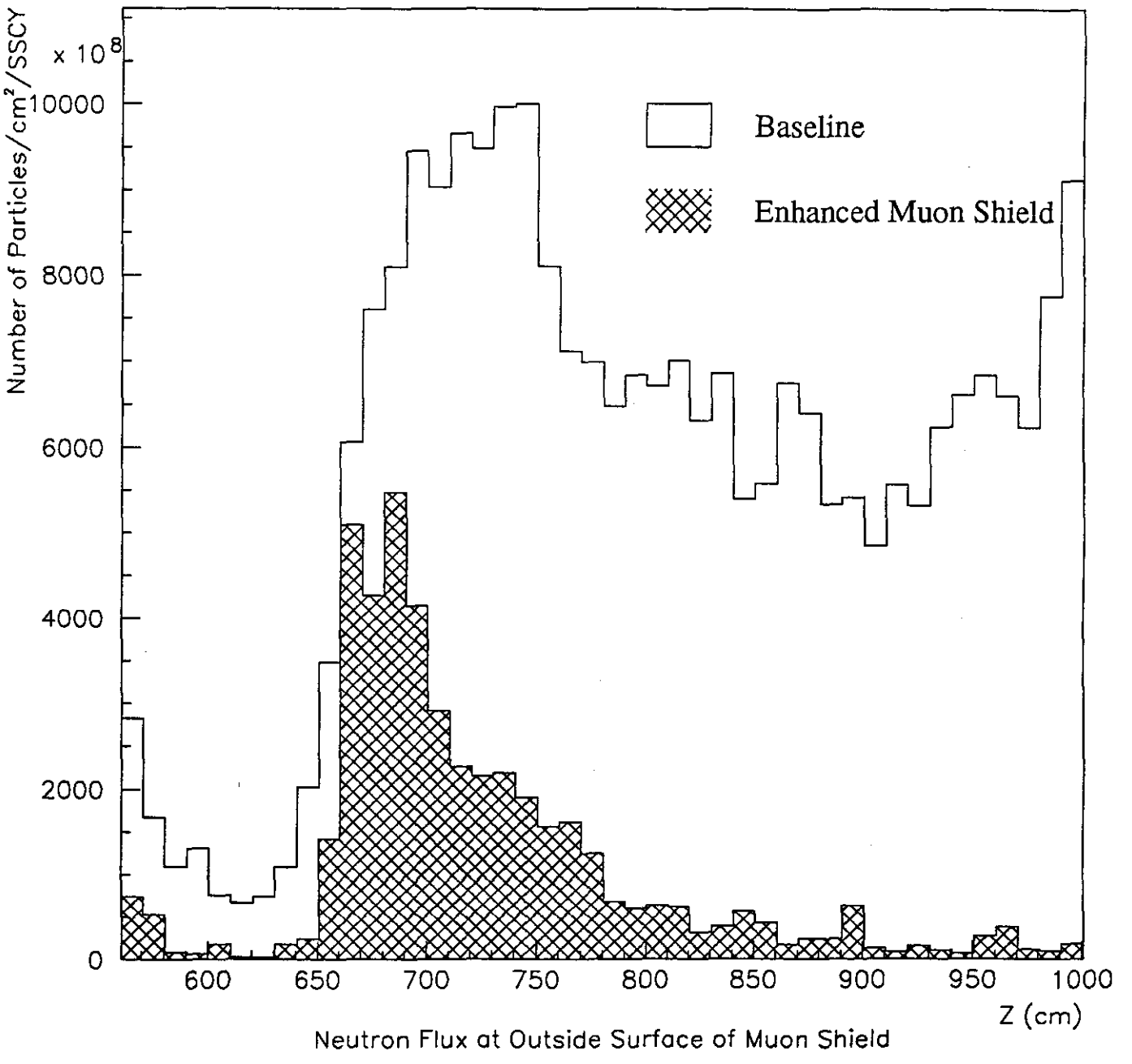
Number of Particles/cm²/SSCY
x 10⁸
10000
8000
6000
4000
2000
0
600
650
700
750
800
850
900
950
1000
Z (cm)
Baseline
Enhanced Muon Shield
Neutron Flux at Outside Surface of Muon Shield

FIGURE 4

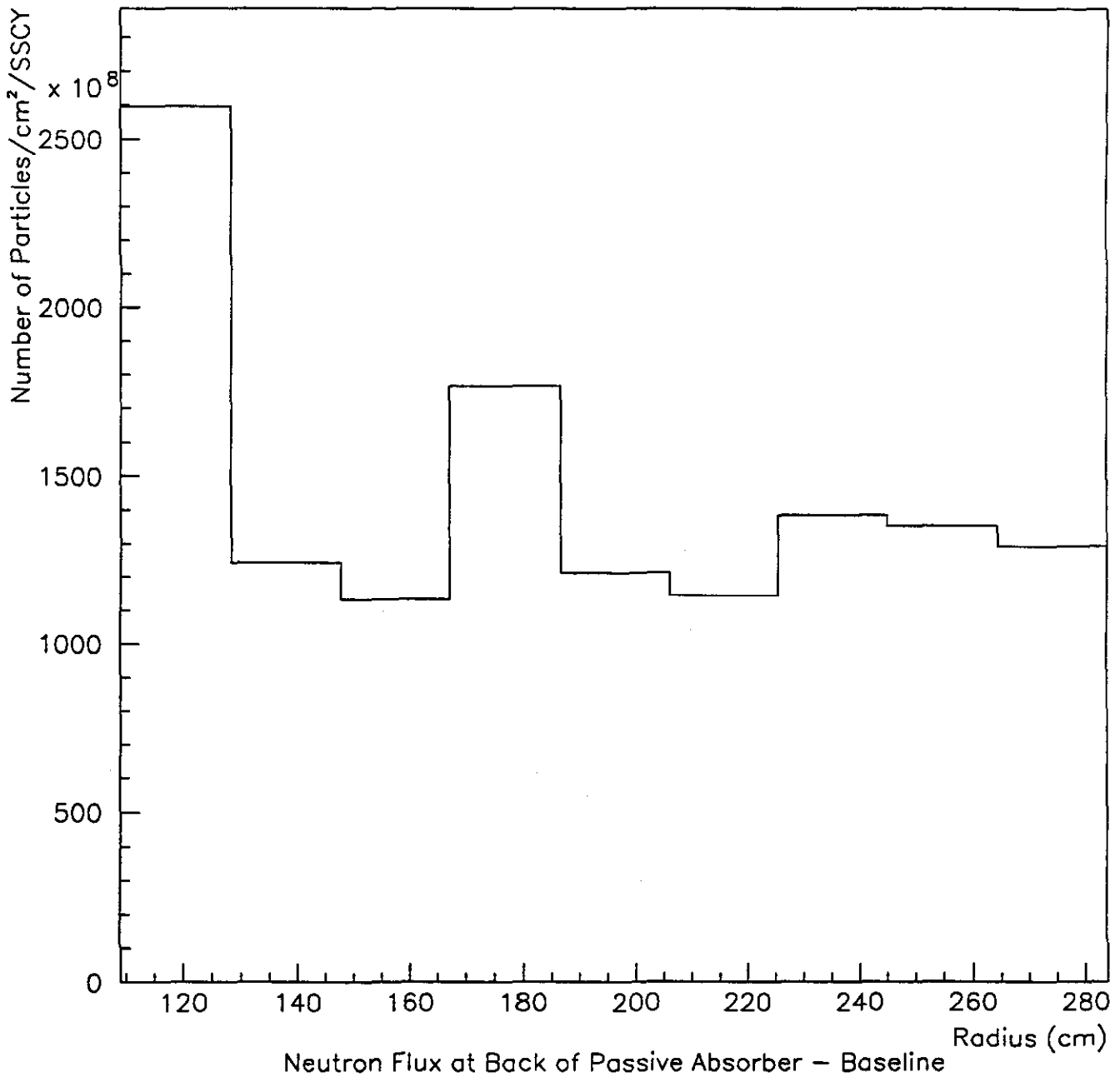
Number of Particles/cm²/SSCY
x 10⁸
2500
2000
1500
1000
500
0
120
140
160
180
200
220
240
260
280
Radius (cm)
Neutron Flux at Back of Passive Absorber – Baseline

FIGURE 5

Fig. 6. Only the PA and some neighboring material was used in the simulation to check punchthrough of neutrons for the passive absorber. Source particles were taken to be those neutrons that are crossing the inside surface of the PA (which is also the outside surface of the outer cryostat wall) in the baseline run, as well as those crossing outward at the inner radius of the PA (which mostly is also the outer radius of the FHAC). In all the runs except two, a ring of material was in place against the back wall and outer flange of the PA. This ring was 14.8 cm thick in the Z-direction and had a radial thickness of 30 cm. The inner corners of the muon chambers are shown at the bottom of the diagram, and we see that the ring is some distance away from the muon chambers and could perhaps be made even bigger. The beam pipe, being "far from the action", has been left out of the simulation to simplify the geometry setup. Air fills the region where the inside of the beampipe would be.

The neutrons and photons punching through the PA were scored according to the likelihood of a given particle type of creating a signal in the inner superlayer of forward muon chambers. On page 4-22 of the GEM Technical Design Report, it is shown that the relative efficiencies in the inner superlayer of the FMC's for neutrons above 100 keV, neutrons below 100 keV, and gammas are 1.0, 3.25, and 21.5, respectively. I applied this weighting to the escaping particles to arrive at a figure of merit – lower numbers indicating those combinations of materials and thicknesses that produce the fewest signals in the muon chambers. Presumably, a configuration with a figure of merit double that of some other configuration will allow twice the signals in the forward muon chambers than the other, at least in the inner superlayer.

Results are shown in Table 1. The thicknesses are as measured at the upper part of the PA and do not include the block in the corner nor the air that represents an electrical junction box, and thus always add to 48.2 cm. These thicknesses exclude the block in the corner. The thicknesses in the PA flange which lies against the FHAC are proportional to the given thicknesses for the upper part, and these will sum to 25.3 cm.

The first run was for the baseline copper with no ring sitting in the corner of the PA and the PA flange. The second line is the same with the ring in place. Putting this ring in the corner where the PA punchthrough flux is the greatest decreases the neutron punchthrough by almost 25% and the photon punchthrough by about 50%. Overall, the

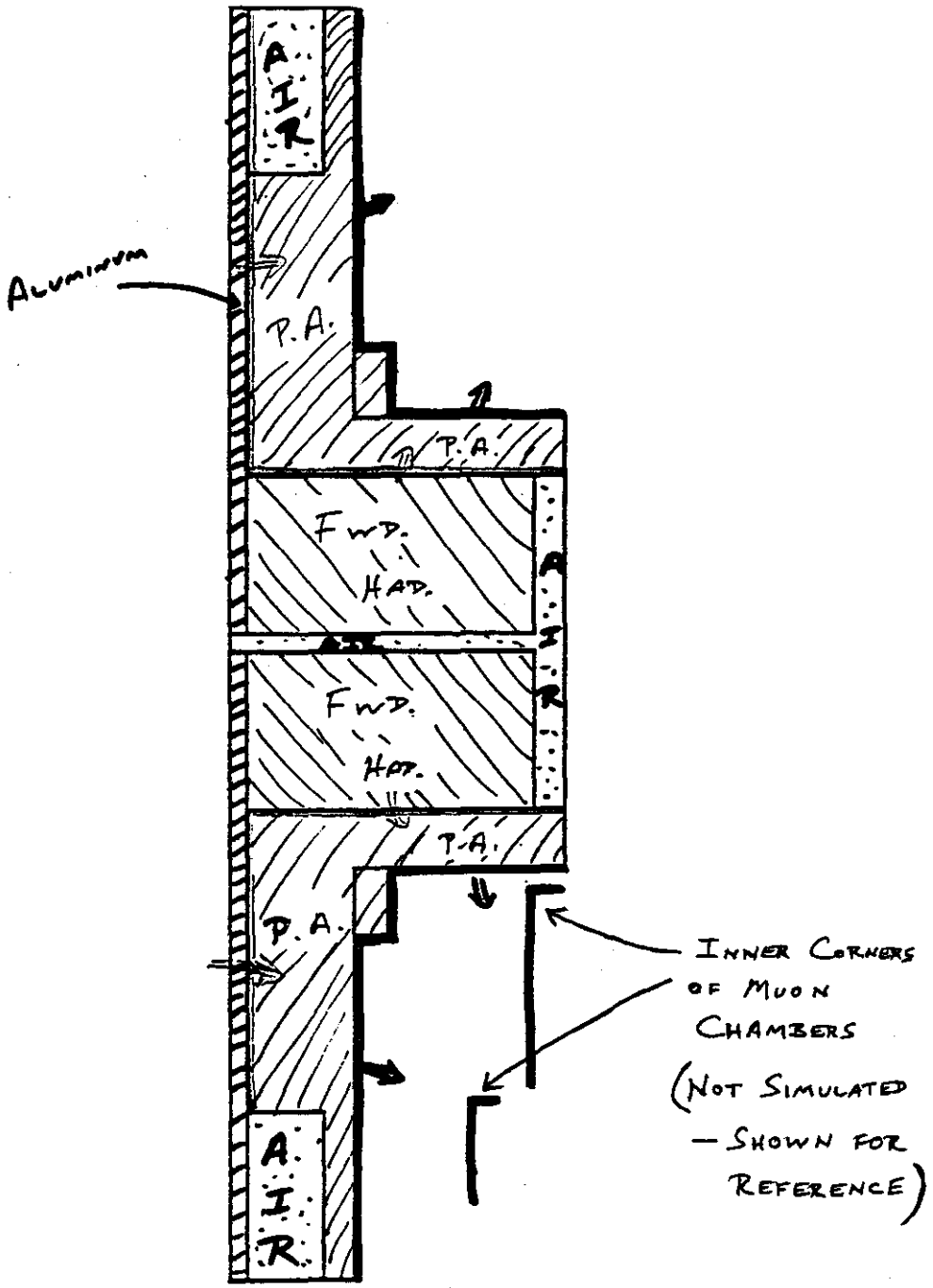

SABRINA Picture of Geometry Simulated
for Passive Absorber Punchthrough Optimization

FIGURE 6

Results of Passive Absorber Optimization Simulations

Material – Thickness	n (E > 100 keV)	n (E < 100 keV)	Total n	Total γ	Figure of Merit
Copper – No Block	551	209	760	30	1,869
Copper – Block	399	186	585	14	1,311
Barite – No Block	462	213	675	266	6,876
Barite – Block	419	199	617	43	1,996
Borated Polyethylene	455	16	471	6,364	137,323
Copper – 34.2 Barite – 14.0	207	233	439	57	2,184
Copper – 14.0 Barite – 34.2	307	181	487	45	1,860
Copper – 41.2 B. Poly. – 7.0	162	88	250	360	8,183
Copper – 34.2 B. Poly. – 14.0	127	27	153	596	13,027
Copper – 24.1 B. Poly. – 24.1	176	12	187	842	18,312
Copper – 14.0 B. Poly. – 34.2	239	11	250	969	21,098
Copper – 14.0 Barite – 20.2 B. Poly. – 14.0	236	10	246	456	10,077
Copper – 14.0 B. Poly. – 20.2 Barite – 14.0	302	118	420	55	1,876
Copper – 34.2 B. Poly. – 11.0 Copper – 3.0	197	35	232	82	2,073
Copper – 31.2 B. Poly. – 14.0 Copper – 3.0	151	21	172	109	2,560
Copper – 34.2 B. Poly. – 8.0 Copper – 6.0	211	80	291	44	1,413
Copper – 31.2 B. Poly. – 11.0 Copper – 6.0	182	28	210	20	710

TABLE 1

figure of merit is decreased by about 30%. As stated before, it would probably be possible to use a bigger ring without bringing that part of the PA unacceptably close to the muon chambers, allowing a still greater reduction in punchthrough rates. It is clear that adding a ring in this corner provides a significant reduction in particles punching through the PA and I recommend that this be added to the baseline design.

The barite concrete without a block, in the third row, shows a higher figure of merit than the copper baseline, in the first row, due to the punchthrough of gammas. In the fourth row are the results of a simulation using the barite concrete with a block in place. The gammas escaping with the block in place are greatly reduced, by a factor of six, indicating that the escaping gammas in the copper are more spread out than in the barite concrete. I also ran a simulation using the full forward region shown in Fig. 2, in which the copper in the PA was replaced with barite concrete. Results of this simulation are discussed below in §5.

Figs. 7 and 8 show how punchthrough can be reduced as a function of thickness of materials. These show the punchthrough for neutrons, for photons, and the figure of merit for copper/barite and copper/borated polyethylene combinations, respectively, as a function of the copper thickness. The copper is always in front and the other material in back. Note that the vertical scales are different and that the figure of merit is divided by 10 for the copper/barite but by 100 for the copper/borated polyethylene. The neutron punchthrough curves indicate the presence of fairly well-defined minima at a copper thickness of around 30 cm. The photon punchthrough decreases continually in the copper/borated polyethylene case (for all borated polyethylene in Fig. 8 the point is well off the scale), but increases gradually to a maximum then falls off for the copper/barite configurations. In both these cases, the minimum figure of merit is obtained by using all copper (the figure of merit point in Fig. 8 for all copper overlays the photon punchthrough point).

All of the configurations with borated polyethylene in the back yielded large numbers of gammas, which the muon chambers are especially sensitive to, making these configurations totally unacceptable. If one puts some copper behind the polyethylene, however, it can absorb the gammas and produce a desirably small figure of merit. After checking a few different thicknesses for such configurations, the best copper and borated polyethylene 'sandwich' I found was 11 cm of polyethylene between 31.2 cm of copper in front and 6 cm

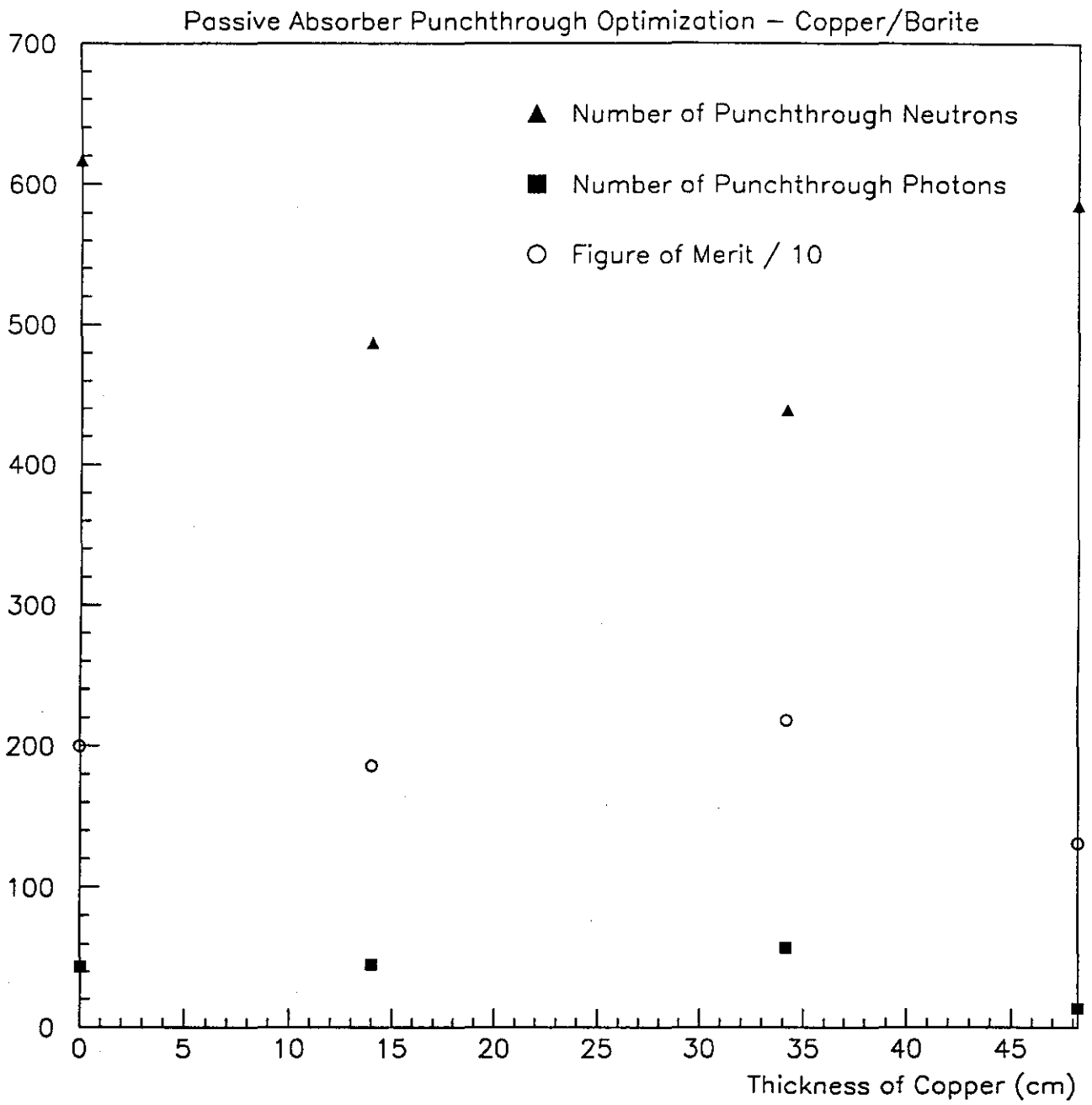
Passive Absorber Punchthrough Optimization – Copper/Barite
Number of Punchthrough Neutrons
Number of Punchthrough Photons
Figure of Merit / 10
700
600
500
400
300
200
100
0
0
5
10
15
20
25
30
35
40
45
Thickness of Copper (cm)

FIGURE 7

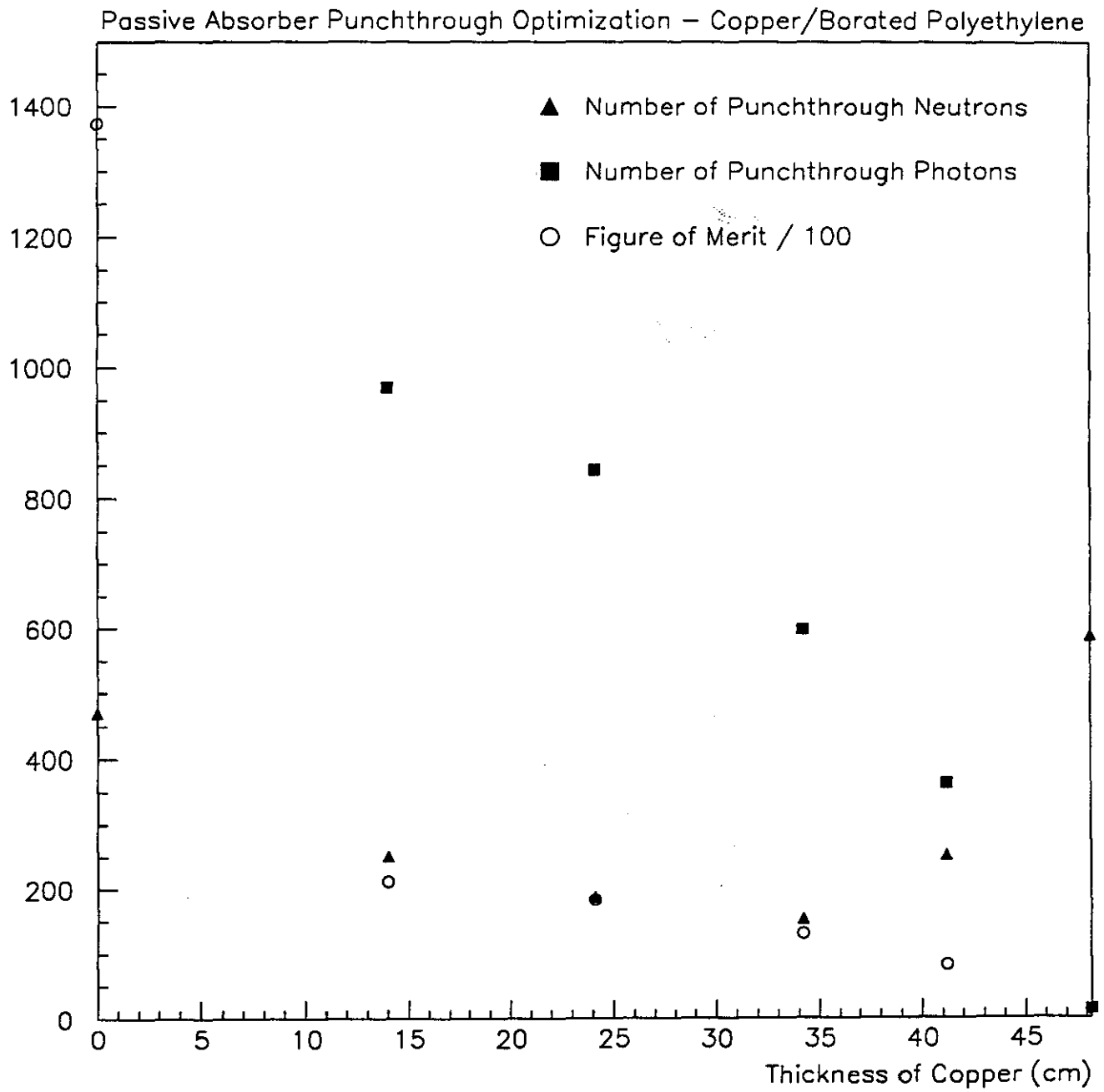
Passive Absorber Punchthrough Optimization – Copper/Borated Polyethylene
Number of Punchthrough Neutrons
Number of Punchthrough Photons
Figure of Merit / 100
1400
1200
1000
800
600
400
200
0
0
5
10
15
20
25
30
35
40
45
Thickness of Copper (cm)

FIGURE 8

of copper behind. The figure of merit of 710 was the lowest obtained – just a little over half that of the next lowest, which was the pure copper. Though the number of gammas leaking was comparable to copper, this combination was particularly effective at stopping both high and low energy neutrons. Further optimization of the thicknesses of these layers could reduce the figure of merit even more.

Considering Fig. 3 shows that PA punchthrough is easily the lowest source of neutrons escaping into the FMC region, even in the shielded case, it is not clear whether a reduction of 50% in the figure of merit for passive absorber punchthrough would be worth the extra cost, in terms of engineering and materials, to justify building a Cu-B.Poly.-Cu sandwich. As for optimizing such a sandwich, a series of simulations could be run to conduct a full two-dimensional parameter search to minimize the figure of merit as a function of the positions of two interfaces instead of just one, as was done in Figs. 7 and 8. I am willing to conduct such simulations to further optimize the thicknesses in a Cu-B.Poly.-Cu PA and the size of the corner block to use, if sufficient interest is shown by the rest of the collaboration. It appears certain that having the block in place is worthwhile.

5. Neutron Escapes through the Cryostat Vacuum Gap

With the improved shield between the PA and FFS, the largest source of neutrons escaping into the FMC area come from escapes out the cryostat vacuum gap. As one possibility in cutting down on this source of leakage, I replaced five centimeters of copper at the front surface of the PA, right up against the outside of the outer cryostat wall, with borated polyethylene. Table 2 summarizes the results. These are from the regional simulations that include the entire forward region, as shown in Fig. 2.

The first column gives the number of neutrons escaping from each area of concern for the baseline while the second lists the same for 5 cm of polyethylene in the PA. The second column is an average of two separate runs. The third column gives the results of using barite concrete in the PA instead of copper. All these runs had the same source particles from DTUJET, but the two runs with the polyethylene used different random number sequences, as did the baseline and barite concrete runs. The 10 cm copper muon shield was used between the PA and FFS in all runs, not the enhanced muon shield with 25.3 cm of copper and the barite concrete wedge.

Neutron Leakage Results for Copper Passive Absorber,
Polyethylene Lined Passive Absorber,
and Barite Concrete Passive Absorber

	Copper PA	Polyethylene Lined PA	Barite PA
Cryostat Vacuum Gap	4,183	2,856	2,935
Back of Passive Absorber	902	954	719
Shield Between PA & FFS	11,183	12,051	10,758

TABLE 2

Roughly, the polyethylene lining causes the escapes out the cryostat vacuum gap to decrease by a factor of about one-third. The number of escapes from the back of the PA is similar, and the number of escapes through the 10 cm copper muon shield is a little higher. Overall, the reduction in escaping neutrons appears to be 2-3%. If this 5 cm lining were added to the configuration with the enhanced muon shield, and the leakage out the back of the PA and through the muon shield were increased in proportion to the above table, it would further reduce the number of total escaping neutrons as compared to the configuration with the enhanced muon shield by about one-sixth.

Using barite concrete throughout the PA also reduces the escapes out the cryostat vacuum gap by one-third. The number of escapes through the 10 cm copper muon shield is not significantly lowered, but the punchthrough for the PA drops by about 20%. Overall, the number of neutrons escaping drops about 10%. In particular, low-energy neutrons escaping from the cryostat vacuum gap are reduced by one-third (most of the neutrons escaping the vacuum gap are below 100 keV), and the high-energy punchthrough neutrons are decreased by about one-third while the number of low-energy punchthrough neutrons are unchanged. That the low-energy neutrons escaping the cryostat vacuum gap should be so decreased in number is expected.

We can compare this result with the findings above from §3, which simulations used only the passive absorber, outer cryostat wall, and forward hadronic calorimeter. In that

simulation, it was found that punchthrough for a barite concrete PA as compared to a copper PA was about 10% lower for neutrons of all energies, whereas it was 20% lower in this simulation. The number of gammas escaping, however, was seen to be so large as to make a totally barite concrete PA undesirable in terms of punchthrough.

I believe a borated polyethylene lining at the front of the PA is worth considering and should be studied in a global simulation to verify the magnitude of the improvement in leakage, particularly since my simulation does not indicate how many of the neutrons escaping through the cryostat vacuum gap actually make it to the FMC region. Many may be absorbed by the scintillating barrel calorimeter or reflected elsewhere, thus diminishing the value of this change. Engineering issues and the increased cost of producing a more complicated PA are also a concern, and more study might help to insure that the benefit justifies the expense.

6. Summary

To minimize the neutron leakage from the forward region of the detector into the area where the forward muon chambers are, I have studied using an enhanced muon shield between the passive absorber and the forward field shaper, lining the inside of the passive absorber with 5 cm of borated polyethylene, and using a barite concrete passive absorber. To minimize both neutron and gamma punchthrough for the passive absorber I have simulated a variety of configurations using different materials and thicknesses of said materials. Based on these studies, I have the following observations and recommendations to make:

1. An enhanced muon shield between the passive absorber and the forward field shaper which is made of iron and barite concrete has been proposed and incorporated into the current baseline design with the shape of the barite concrete modified as indicated in Fig. 12-1 of the GEM Technical Design Report. My simulations confirm the need for this enhanced shield, indicating that it should reduce the neutrons escaping into the region where the forward muon chambers are by about 60%.

2. A ring of material should be positioned in the corner of the passive absorber against the passive absorber flange to reduce neutron and gamma punchthrough of the passive absorber. The muon group should be consulted to find out how near the inner superlayer of muon chambers this ring can be.

3. If it is feasible in terms of engineering and cost, the passive absorber should be a sandwich of copper, borated polyethylene, and copper in order to reduce further the passive absorber punchthrough. Although the optimal thicknesses of these materials is not certain, 31.2 cm, 11.0 cm, and 6.0 cm, respectively, appears to be a good starting point. I will work on further optimizing these thicknesses if interest warrants. I also recommend that this configuration be simulated in one of the global packages to assure that the reductions are significant before it is adopted.

4. Placing 5 cm of borated polyethylene at the front of the passive absorber may be helpful to reduce the leakage of neutrons through the cryostat vacuum gap. Again, I recommend that this possible change be incorporated into a global simulation to gauge how many of the neutrons escaping from this chimney actually make it into the region where the muon chambers are, and, thus, whether it is worth making this change in the design.

Acknowledgments

I would particularly like to thank Milind Diwan, head of the GEM Neutron Task Force, for his help and advice. I would like to acknowledge the contributions to this project of other members of the task force: Yuri Fisyak, who came up with the ideas for solving a number of the shielding problems; Nikolai Mokhov, who provided the DTUJET events; and Laurie Waters, for helpful discussions and for helping me get a copy of the SABRINA package, which generates pictures of the detector as set up using the combinatorial geometry description files and helps to find errors that may be in them. Thanks also to Group B of the SSC for allowing me to visit the SSC Laboratory for two months to work on this project. This work was also supported by the Texas National Research Laboratory Commission and the United States Department of Energy through grant number DE-FG05-91ER40622.